Atomization of Liquids by Two-phase Gas-liquid Flow through a Plain-orifice Nozzle: Flow Regimes inside the Nozzle

By *Marc Lörcher* and *Dieter Mewes**

Liquids or suspensions are divided into sprays of small droplets by atomization of two-phase gas-liquid mixtures. In this way either an equal distribution of the droplets or the generation of large surface areas of the liquid phase are accomplished, leading to increased heat- and mass-transfer. The spatial and time dependency of the mean droplet diameter is a function of the total pressure upstream of the nozzle, the volumetric flow rate of the liquid and the gas, as well as on the flow regime in the nozzle. Thus the radial and axial profile of the void fraction inside the nozzle are measured with an electrical measurement technique. In addition, the flow in the nozzle is imaged by a high-speed camera. Three flow regimes are identified. These are bubbly flow, plug flow and annular flow. A continuous flow of the emitting spray is observed for bubbly flow and annular flow only. The distribution of the dispersed bubble phase is given by ratio of the isothermic compression energy needed to pressurize the gas mass flow rate from atmospheric pressure up to the total pressure in front of the nozzle, and the potential energy of the supplied liquid mass flow rate.

1 Introduction

A spray of small droplets is formed by the atomization of a liquid or a suspension in two-phase nozzles. The goal is either the equal distribution of the droplets, or the generation of large surface areas of the liquid phase in order to increase the heat- and mass-transfer in the spray. In two-phase gas-liquid nozzle flow, the pressurized gas phase is dispersed within the liquid phase. The two-phase mixture passes a short tube and is accelerated to critical mass flow conditions by reducing the cross-section. Beyond the narrowest cross section where critical mass flow is observed, the gas flow expands and the liquid is dispersed into filaments. The filaments decompose into droplets, where the spatial and time dependencies of the mean droplet diameter are a function of the total pressure in front of the nozzle, the volumetric flow rate of liquid and gas, as well as on the flow regime inside the nozzle. Buckner and Sojka [1] investigate the drop size in sprays of fluids with viscosities between $0,4\,\mathrm{Pa}\cdot\mathrm{s}$ and $1,0\,\mathrm{Pa}\cdot\mathrm{s}$[1)]. The mean droplet diameter is a strong function of the air-liquid ratio and nearly independent of liquid viscosity, fluid supply pressure and mixture mass flow rate. Lefebvre, Wang and Martin [7] and Whitlow and Lefebvre [24] investigate the Sauter-mean-diameter and the Rosin-Rammler distribution parameter for the drop size in sprays produced at various air-liquid ratios and total pressures in front of the nozzle. Roesler and Lefebvre [20,21] investigate sprays at extreme low air-liquid ratios. Lund, Sojka, Lefebvre and Gosselin [10] present experimental results of drop size measurements in sprays of liquids with various surface tension. They calculate the Sauter-mean-diameter and compare the results with experimental. Lund, Jian, Sojka, Gore and Panchagnula [11] investigate the influence of the atomizing gas molecular weight on the Sauter-mean-diameter, the Rosin-Rammler distribution parameter and the average velocity. The spray cone angle is observed in dependency of the surface tension and the liquid viscosity by Chen and Lefebvre [6]. Luong and Sojka [12] discuss the unsteadiness of droplet size, velocity and arrival time in sprays. They found that the unsteadiness is influenced by the air-liquid ratio, the liquid mass flow rate and the physical properties of the liquid. The entrainment in sprays at low mass flow rates is analysed by Bush and Sojka [2] and Ricou and Splading [19]. Raetzo [14] compared the spray characteristics of an external- and an internal-mixing twin-fluid nozzle and apressure swirl nozzle. Chen and Lefebvre [5] present a model to calculate the atomized mass flow rate in dependence of the air-liquid ratio and the pressure in front of the nozzle. Chawla [3,4] studies the atomization of two phase mixtures with critical mass flow rates and establishes a model to calculate the critical mass flow density. Nevertheless there was no investigation done which addresses the different flow regimes inside the nozzle. There is also no information found about the context between the flow regime inside the nozzle and the characteristics of the resulting sprays. In the present work the experiments are performed with a nozzle, into which the gas and the liquid flow are fed. The total pressure in front of the nozzle is varied in the different experiments ($p_0 < 1.6\,\mathrm{MPa}$). The liquid is atomized to be ambient, no pressurized chamber is used. A schematic of this nozzle is

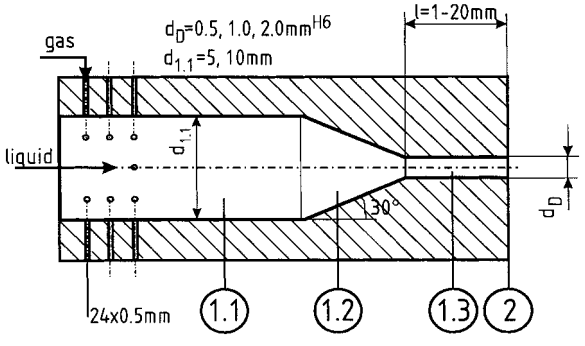

Figure 1. Schematic diagram of the nozzle: 1.1 mixing chamber, 1.2 conical part, 1.3 discharge section, 2 exit cross section.

[*] Dipl.-Ing. M. Lörcher, Prof. Dr.-Ing. D. Mewes, Institut für Verfahrenstechnik der Universität Hannover, Callinstr. 36, D-30167 Hannover, Germany; e-mail: dms@c36.uni-hannover.de

1) List of symbols at the end of the paper.

  0930-7516/01/0202-0167 $ 17.50+.50/0

presented in Fig. 1. The temperature, pressure and mass flow of both phases are measured at the entrance of the nozzle. The radial profile of the void fraction inside the nozzle is measured with an electrical tomographic measurement technique by Lörcher, Schmitz and Mewes [9]. The axial profile of the void fraction is measured by a similar measurement technique. A decision about the flow regime is done by a statistical analysis of the axial profiles.

2 Classification of Modes of Disintegration

Rayleigh [15], Taylor [22], Weber [25] and Ohnesorge [13] investigated the disintegration of liquid jets and identified several regimes of drop formation. Three physical mechanisms are described.

- Rayleigh mechanism of breakup: Oscillations causes jet breakup, dilational, radially symmetric waves.
- Wave-like breakup caused by air fraction, sinuous waves. Aerodynamic forces overcome surface forces.
- Atomization: Chaotic, irregular disintegration.

The different regimes are plotted in Fig. 2 in the form of Ohnesorge's chart. Since for a given liquid and orifice size the Ohnesorge number is constant, the variation of the breakup regime can be achieved only by increasing the liquid velocity at the exit cross section. In two-phase atomization the breakup regime is not only influenced by the flow of the liquid but also by the gas flow. Therefore Ohnesorge's chart is complemented in Fig. 3 by a third axis for the Reynolds number of the gas flow. Atomization of a given liquid flow and preselected orifice size is no longer calculated along a straight line (Fig. 2), but rather represented by a plane (e.g., the gray colored plane in Fig. 3) for a diameter of 1mm and water as the atomized liquid. For critical flow of the gas-liquid mixture the individual phase flows cannot be varied independently from each other. Critical flow is only observed along a single bended line in the described gray plane. The Reynolds number of the liquid at the exit cross section is defined as

$$Re_l = \frac{j_l\, d_D\, \rho_l}{\eta_l} \tag{1}$$

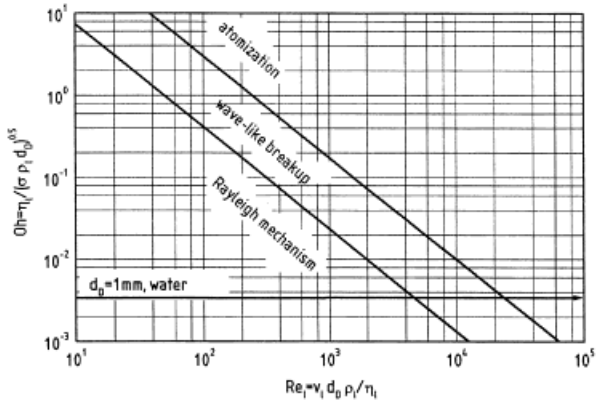

Figure 2. Modes of disintegration in the classification of Ohnesorge.

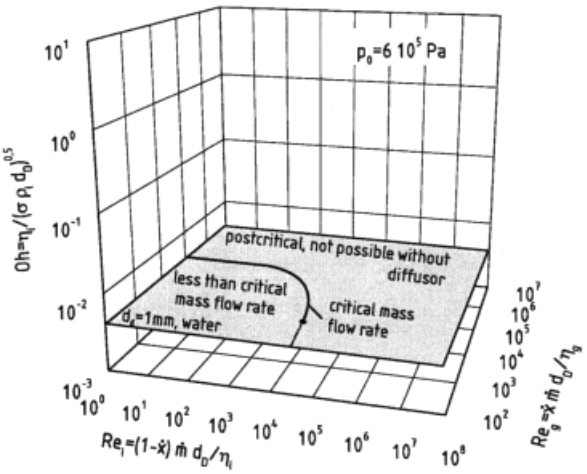

Figure 3. Modified diagram of Ohnesorge for the atomization by two-phase gas-liquid flow.

where j_l is the superficial velocity of liquid in the exit cross section, and d_D is the diameter of the exit cross section. With the limitation of critical flow, the Reynolds number of the liquid flow is

$$Re_l = \frac{\dot{m}_c\,(1-\dot{x})\,d_D}{\eta_l} \tag{2}$$

where $\dot{m}_c$ is the critical mass flow density in the exit cross section, and $\dot{x}$ is the gas mass flow fraction of the two phase flow. Similarly, the Reynolds number of gas flow in the exit cross section is

$$Re_g = \frac{\dot{m}_c\,\dot{x}\,d_D}{\eta_g} \tag{3}$$

Along the single bended line in the plane shown in Fig. 3, the total pressure upstream of the nozzle is constant and the gas mass flow fraction is varied. The critical mass flow density is calculated as a function of the total pressure in front of the nozzle and the gas mass flow fraction. Different calculation methods are evaluated. The frozen flow model from Leung and Epstein [8] was found to be the most suitable. For low Reynolds numbers of the liquid flow, the gas mass flow fraction is high and decreases along the depicted curve. By this the atomized mixture becomes increasingly more wet. At a certain point the corresponding pressure after acceleration to critical velocity and before the expansion is reduced to that of the surrounding atmospheric pressure, and as the atomized mixture becomes wetter, critical mass flow is no longer possible. The experimental work is done in order to obtain a relation between the flow regimes inside the nozzle, and the integral flow parameters of gas and liquid flow as well as the resulting spray. As a first step, the correspondence between the integral flow parameters and the flow regimes inside the nozzle are shown. Also regions for different flow regimes in the mixing chamber are drawn into the chart (Fig. 4). There are regions for bubbly flow, plug flow and annular flow. The regions are separated by transients. The flow regimes depend

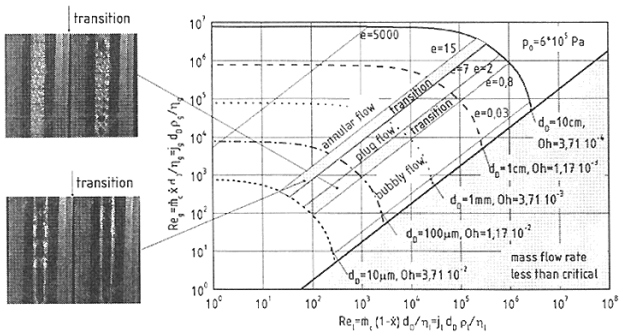

Figure 4. Gas Reynolds number as a function of the liquid Reynolds number for critical mass flow.

on the energy ratio between gas and liquid flows. The energy ratio e is defined as the ratio of the isothermic compression energy needed to pressurize the gas mass flow rate from atmospheric pressure to the total pressure in front of the nozzle, to the potential energy of the supplied liquid mass flow rate

$$e = \frac{\dot{M}_g \frac{p_\infty}{\rho_{g,\infty}} ln(\frac{p_0}{p_\infty})}{\dot{M}_l \frac{p_0 - p_\infty}{\rho_l}} \tag{4}$$

The mass flow rates of gas and liquid can be written as

$$\dot{M}_g = \dot{m}_c \cdot A_D \cdot \dot{x} \tag{5}$$

$$\dot{M}_l = \dot{m}_c \cdot A_D \cdot (1 - \dot{x}) \tag{6}$$

where $\dot{m}_c$ is the critical mass flow density and A_D is the cross section of the exit orifice. Using the expressions for the mass flow rates of gas and liquid, Eq. 4 can be transformed as

$$e = \frac{\dot{x}}{(1-\dot{x})} \frac{p_0 - p_\infty}{p_\infty} \frac{\rho_l}{\rho_{g,\infty}} ln\left[\frac{p_0}{p_\infty}\right] \tag{7}$$

Thus the energy ratio depends on the gas mass flow fraction $\dot{x}$ and the total pressure in front of the nozzle p_0. In Fig. 4 the total pressure in front of the nozzle is constant. Eq. 7 states that for constant energy ratios the gas mass flow fraction is constant. From Eq. 2 one can express d_D in terms of Re_l, and substitute this form into Eq. 3 to get the relation

$$Re_g = \frac{\dot{x}}{1-\dot{x}} Re_l \frac{\eta_l}{\eta_g} \tag{8}$$

Therefore, straight lines represent constant energy ratios in the modified Ohnesorge chart (Fig. 4). Different flow regimes may be described by the energy ratio.

3 Axial Profiles of the Void Fraction

Different flow regimes can be recognized in the nozzle by the detection of single short plugs and bubbles covering the whole cross section. In the axial direction, 10 wires are placed inside the nozzle at a distance of 2 mm each. Either the conductance between the 9 pairs of neighbouring wires is measured with about 1000 Hz, or the conductance between a pair of only two wires is measured with frequencies of about 4000 Hz. The measured conductance is a function of the distribution of the water and the air flow between each two wires. Depending on the flow pattern, the wires are electrically connected by different amounts of liquid. This corresponds to a parallel arrangement of electrical resistors as shown in Fig. 5.

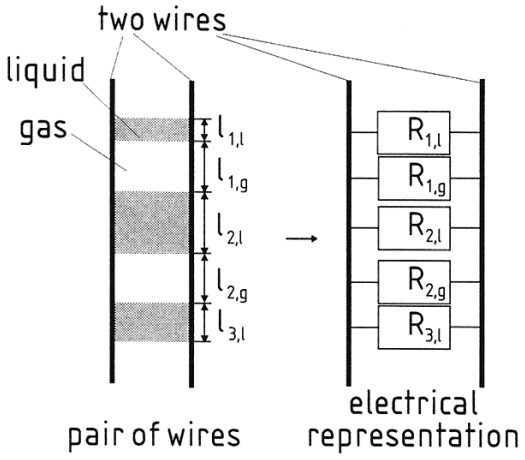

Figure 5. Distribution of the liquid between two wires and its electrical expression.

With a negligible air conductance, the measured conductance is

$$G_M = \sum_{i=1}^{n} \frac{1}{R_i} \tag{9}$$

where R_i is the resistance of one liquid-filled area between two wires. The resistance of one liquid-filled area of length l_i can be calculated according to

$$R_i = \frac{1}{G_{max}} \frac{l_{max}}{l_{i,l}} + \frac{1}{G_{min}} \frac{l_{max}}{l_{i,g}} \tag{10}$$

where l_{max} is the maximum possible length of areas filled with liquid between two wires (usually the length of the wires inside the mixing chamber). G_{max} is the maximum conductance that follows when the wires are completely wet and G_{min} is the conductance when the wires are completely dry. From the Eqs. 9 and 10 follows the measured conductance

$$G_M = G_{max} \sum_{i=1}^{n} \frac{l_{i,l}}{l_{max}} + G_{min} \sum_{i=1}^{n} \frac{l_{i,g}}{l_{max}} \tag{11}$$

which can be expressed as

$$G^* \equiv \frac{G_M - G_{min}}{G_{max} - G_{min}} = \frac{\sum_{i=1}^{n} l_{i,l}}{l_{max}} \tag{12}$$

where G^* is the relative conductance with a value between 0 and 1, and is equal to the liquid fraction $1 - \alpha$.

The measured void fraction is shown for one pair of wires in Fig. 6. For bubbly flow the void fraction is relatively low and oscillates with a high amplitude around the mean value. Short plugs with low void fraction and long regions with a constant high void fraction are detected for plug flow. For annular flow

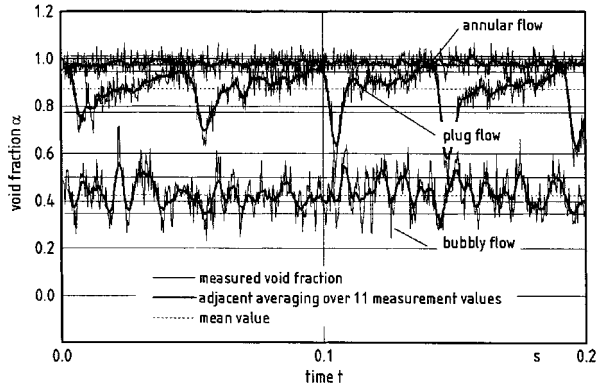

Figure 6. Measured void fraction between two wires for bubbly flow, plug flow and annular flow as a function of the time.

the void fraction is close to one and the oscillation around the mean value is small. Although the flow regimes are easy to identify in this chart, a decision about the actual regime is not necessarily objective, especially in the transition regions between the different flow regimes. Therefore, a statistical criterion must be found to analyse the current flow regime from the measured axial profile of the void fraction. Therefore the measured void fractions are presented as a function of time (Fig. 6), and this same data is also expressed by the probability density function (pdf) of occurrence as a function of the void fractions (Fig. 7). For bubbly flow, the distribution of the pdf is symmetric and relatively wide. The distribution for plug flow is no longer symmetric because the short plugs are infrequent and have a low void fraction. For annular flow, the distribution is again symmetric and more narrow. Statistically, the expression for the asymmetry of the pdf can be defined by a ratio of the third and the second central moments of the distribution with

$$g \equiv \frac{m_3(\bar{\alpha})}{m_2(\bar{\alpha})^{3/2}} \tag{13}$$

$$g \equiv \frac{\frac{1}{n}\sum_{i=1}^{n}(\alpha_i - \bar{\alpha})^3}{\left[\frac{1}{n}\sum_{i=1}^{n}(\alpha_i - \bar{\alpha})^2\right]^{3/2}} \tag{14}$$

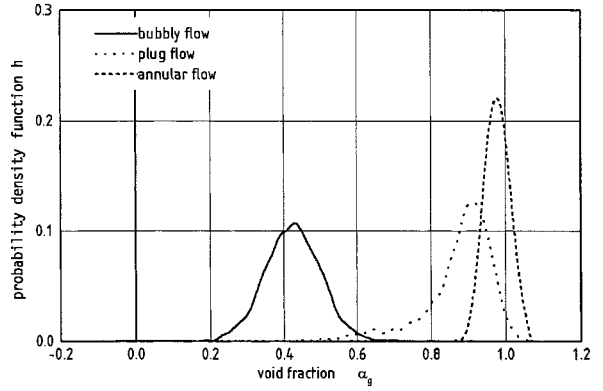

Figure 7. Frequency of occurrence for bubbly flow, plug flow and annular flow as a function of the void faction.

where $\bar{\alpha}$ is the mean value of all measured void fractions and α_i is the i-th void fraction of one experiment. This expression for the asymmetry is calculated for several experiments performed at different total pressures in front of the nozzle and different gas mass flow fractions. In Fig. 8 the asymmetry is shown as a function of the energy ratio. For low energy ratios the asymmetry is about zero, and the distribution of the frequency of occurrence is symmetric. For higher energy ratios the asymmetry becomes negative and the distribution leans toward higher void fractions. If the energy ratio is increased further the asymmetry is again near zero, in the annular flow regime. The measured values follow the depicted curve. The three flow regimes correspond to the horizontal lines, between which the transition regions are found. The values of the energy ratio at the end of the horizontal lines are taken to define the transition regions in Fig. 4. The measurement of the void fraction, and the calculation of the asymmetry from the measured void fraction, are fully reproduceable and provide an objective criterion which can discern between the different flow regimes.

The length of the channel inside the nozzle is short. Therefore the velocity profile is not completely developed at the outlet. As a result, the flow regime at the exit cross section is not independent from the mechanisms the gas is dispersed into the liquid. In Fig. 9 the asymmetry is shown as a function

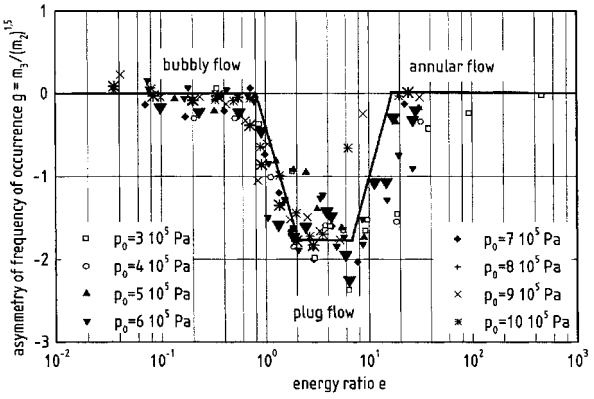

Figure 8. Asymmetry of the distribution of the void fraction as a function of the energy ratio; central moment of order r: $m_r = m_r(\bar{\alpha}) = \frac{1}{n}\sum_{i=1}^{n}(\alpha_i - \bar{\alpha})^r$.

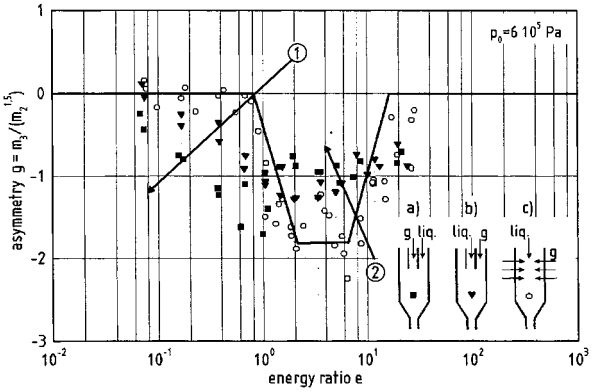

Figure 9. Asymmetry as a function of the energy ratio for different units of the gas integrator.

of the energy ratios for modified gas integrator units. The gas is dispersed through 24 holes with 0.5 mm diameter located along three rings with 8 holes each (gas integrator c). In gas integrator a, the liquid is axially fed through a ring into the nozzle and the gas is also axially fed into the center of this ring. In the experiments it was found that plug flow (Fig. 9, arrow 1) in gas integrator unit is observed at lower energy ratios than with the gas integrator unit c. At higher energy ratios (e = 2...8), the calculated asymmetry in unit is less than for the gas integrator unit (Fig. 9, arrow 2). For this range of energy ratios, less pulsation of the spray is observed.

4 Critical Mass Flow

The two-phase mass flow supplied to the nozzle increases when the pressure downstream of the nozzle is reduced. The mass flow increases to a maximum value. If the pressure is further reduced the mass flow remains constant. The maximum value of the mass flow is called critical value. The mass flow at the exit cross section is critical when the atomizer is working properly. The gas mass flow fraction and the total pressure upstream of the nozzle are calculated in order to predict the size and the velocity of the droplets. The critical mass flow rate at the exit cross section is calculated with the model from Leung and Epstein [8]. In the model, frozen flow inside the nozzle is assumed. The mass flow rate depends on the total pressure in front of the nozzle and on the gas mass flow fraction. The measured mass flow rate varies less than 10% from the calculated mass flow rate for the investigated conditions of the total pressure and the gas mass flow fraction.

5 Conclusions

In atomizing liquids by two-phase gas-liquid flow, the spatial and the time distribution of the mean droplet diameter of the spray depend on the total pressure in front of the nozzle, the volumetric flow rate of the liquid and the gas, as well as on the flow regime inside the nozzle. An electrical measurement technique is presented for the axial profile of the void fraction with a high time resolution. The determination of the flow regime is done by a statistical analysis of the measured axial profile of the void fraction. The flow regimes depend on the energy ratio, defined as the ratio of the isothermic compression energy needed to pressurize the gas mass flow rate from atmospheric pressure to the total pressure in front of the nozzle, and the potential energy of the supplied liquid mass flow rate.

Acknowledgement

The authors wish to thank the German Research Foundation (DFG) for their financial support.

Symbols used

$\dot{M}$	$[\frac{kg}{h}]$	mass flow
$\dot{m}$	$[\frac{kg}{m^2 \cdot s}]$	mass flow density
p	[Pa]	pressure
d	[m]	diameter
e	[–]	energy ratio
g	[–]	statistical expression of the asymmetry
G	[S]	conductance
G^*	[–]	relative conductance
h	[–]	relative frequency of occurrence
j	$[\frac{m}{s}]$	superficial velocity
κ	[–]	isentropic exponent
l	[m]	length of wires
$m_r(\bar{\alpha})$	[–]	central moment of order r of the distribution of α
R_i	[Ω]	resistance of area i
T	[K]	temperature
t	[s]	time
v	$[\frac{m}{s}]$	velocity
W	[J]	energy
$\dot{x}$	[–]	gas mass flow fraction

Greek symbols

$\dot{\alpha}$	[–]	gas fraction of volumetric flux
α	[–]	void fraction
ρ	$[\frac{kg}{m^3}]$	density
σ	$[\frac{N}{m}]$	surface tension

Indices

0	upstream of the nozzle
1	inside the nozzle
2	after acceleration to critical velocity and before the expansion
3	in the spray
∞	far away from the nozzle
2ph	two-phase
c	critical
D	smallest cross section of the nozzle
g	gas
i	index of area between two wires
l	liquid
max	maximum value when the maximum area is filled with liquid
min	minimum value when the maximum area is filled with gas
M	measured in the direction M

References

[1] H.N. Buckner; P.E. Sojka, Effervescent Atomization of High-Viscosity fluids: Part I, Newtonian Liquids; *Atomization and Sprays*, *1* (1991) pp. 239–252.

[2] S.G. Bush; P.E. Sojka, Entrainment by Effervescent Sprays at Low Mass Flow Rates; *FED-Vol. 178/HTD-Vol.270, Fluid Mechanics and Heat Transfer in Sprays*, ASME (1993) pp. 117–121.

[3] J.M. Chawla, Atomization of Liquids Employing the Low Sonic Velocity in Liquid/Gas Mixtures; ICLASS-85.

[4] J.M. Chawla, Flüssigkeitsinhalt in Rohren für Flüssigkeits/Gas-Gemische bei der Zweiphasenströmung; *Chem. Ing. Tech.*, *41* (1969) 5+6 pp. 328–330.

[5] S.K. Chen, A.H. Lefebvre, Discharge coefficients for Plain-orifice Effervescent Atomizers; *Atomization and Sprays 4* (1994) pp. 275–290.

[6] S.K. Chen; A.H. Lefebvre, Spray Cone Angles of Effervescent Atomizers; *Atomization and Sprays 4* (1994) pp. 291–301.

[7] A.H. Lefebvre; X.F. Wang; C.A. Martin, Spray Characteristics of Aerated-liquid pressure atomizers; *J. Propulsion 4* (1988) 4, pp. 293–298.

[8] J.C. Leung, M. Epstein, A Generalized Correlation for Two-phase Nonflashing Homogenous Choked Flow; Transactions of the ASME, *Journal of Heat Transfer* (1990) 112, pp. 528–530.

[9] M. Lörcher; D. Schmitz; D. Mewes, Tomographic Measurement Techniques – Visualization of Multiphase Flows; *Machine Graphics ≈ Vision 8* (1999) 4, pp. 667–679.

[10] M.T. Lund, P.E. Sojka; A.H. Lefebvre, P.G. Gosselin, Effervescent Atomization at Low Mass Flow Rates. PartI: The influence of surface tension; *Atomization and Sprays 3* (1993) pp. 77–89.

[11] M.T. Lund; C.Q. Jian; P.E. Sojka; J.P. Gore; M.V. Panchagnula, The Influence of Atomizing Gas Molecular Weight an Low Mass Flowrate Effervescent Atomizer Performance; *FED-Vol.178/ HTD-Vol. 270, Fluid Mechanics and Heat Transfer in Sprays, ASME* (1993) pp. 123–128.

[12] J.T.K. Luong; P.E. Sojka, Unsteadiness in Effervescent Sprays; *Atomization in Sprays 9* (1999) pp. 87–109.

[13] W. Ohnesorge, Formation of Drops by Nozzles and the Breakup of Liquid Jets; *Z. Angew. Math. Mech. 16* (1936) pp. 355–358.

[14] T. Raetzo, Charakterisierung von Düsen zum Zerstäuben von Flüssigkeiten; Dissertation, ETH Zürich 1995.

[15] Lord Rayleigh, On the Instability of Jets; *Proc. London Math. Soc. 10* (1878) pp. 4–13.

[16] N. Reinecke; M. Boddem; G. Petritsch; D. Mewes, Tomographisches Messen der relativen Phasenanteile in zweiphasigen Strömungen fluider Phasen; *Chem. Ing. Tech. 68* (1996) 11, pp. 1404–1412.

[17] N. Reinecke; G. Petritsch; M. Boddem; D. Mewes, Tomographic Imaging of the Phase Distribution in Two-phase Slug Flow; *Int. J. Multiphase Flow 24* (1996) 4, pp. 617–634.

[18] N. Reinecke; G. Petritsch; D. Schmitz; D. Mewes, Tomographic Measurement Techniques – Visualization of Multiphase Flows; *Chem. Eng. Technol. 21* (1998) 1, pp. 7–18.

[19] F.P. Ricou; D.B. Splading, Measurements of Entrinment by Axisymmetrical Turbulent Jets; *J. Fluid Mechanics 11* (1961) pp. 21–32.

[20] T.C. Roesler, A.H. Lefebvre: Studies on Aerated-liquid Atomization; *Int. J. Turbo and Jet Engines 6* (1989) pp. 221–230.

[21] T.C. Roesler, An Experimental Study of Aerated-liquid Atomization; Ph.D. Thesis, Purdue University, West Lafayette, IN, 1988.

[22] G. I. Taylor, The Function of Emulsion in Definable Filed Flow; *Proc. R. Soc. London Ser. A 146* (1934) pp. 501–523.

[23] S.D. Sovani; P.E. Sojka; Y.R. Sivathanu, Prediction of Drop Size Distributions from First Principles: The Influence of Fluctuations in Relative Velocity and Liquid Physical Properties; *Atomization and Sprays 9* (1999) pp. 133–152.

[24] J.D. Whitlow; A.H. Lefebvre, Effervescent Atomizer Operationand Spray Characteristics; *Atomization and Sprays 3* (1993) pp. 137–155.

[25] C. Weber, Disintegration of Liquid Jets; *Philos. Mag. (London) 11* (1931) 2, pp. 136–159.

